Accepted manuscript (author version)

To appear in:

Iranian Journal of Earth Sciences (Iran J. Earth. Sci.)

E-ISSN: 2228-785X Print ISSN: 2008-8779

Received: 16 June 2025

Revised: 19 September 2025

Accepted: 20 November 2025

DOI: https://doi.org/10.57647/ijes.2027.04881

Original Research

Geochemical evidence from olivine for mantle metasomatism and magma evolution in Eocene basalts, North Ardabil, NW Iran

Solmaz Mohammadrezai[1], Ahmad Jahangiri[1], Luca Caricchi[2], Mohsen Moayyed[1]

[1]Department of Earth Science, University of Tabriz, Tabriz, Iran

[2]Department of Earth Sciences, University of Geneva, Geneva, Switzerland

* Corresponding author: a.jahangiri@tabrizu.ac.ir

Abstract

The Eocene volcanic rocks of north Ardabil, NW Iran, provide valuable insight into the dynamic history of mantle processes and subduction-related magmatism along the Alborz-Azarbaijan magmatic belt. This study combines new petrographic observations, whole-rock geochemistry, and high-precision mineral chemistry, focusing on olivine phenocrysts from pyroxene-phyric basalt, basalt, and trachybasalt. These basalts exhibit porphyritic textures, characterized by a dominant presence of clinopyroxene, olivine, and plagioclase within a fine-grained groundmass. Four distinct olivine types were identified based on size, zoning patterns, and chemical composition, with forsterite (Fo) contents ranging from Fo_{59} to Fo_{92}. Whole-rock geochemical analyses classify the host rocks as High-K subalkaline, characterized by LILEs and LREEs, along with depletion of HFSEs and HREEs, consistent with formation in a subduction-related arc setting. Elevated concentrations of Ni, Ca, and Mn in olivine phenocrysts and whole-rock compositions suggest a mantle source dominated by re-fertilized peridotite, with contributions from pyroxenite. Moreover, geochemical signatures indicate complex mantle metasomatism involving carbonate-

and silicate-rich sediment melts, reflecting heterogeneous metasomatic processes beneath this volcanic field during the Eocene.

Keywords: Volcanic rocks, Olivine, Eocene, Metasomatism , North Ardebil, NW Iran

1. Introduction

Mafic minerals such as olivine are widely used to infer magma composition and mantle source features (Sobolev et al., 2005, 2007; Arndt et al., 2010; De Hoog et al., 2010; Herzberg, 2011; Foley et al., 2013; Cordier et al., 2015; Søager et al., 2015; Giuliani and Foley, 2016; Mollai et al., 2021; Arjmandzadeh et al., 2021). The texture and chemistry of these minerals- such as crystal shape, inclusions, structures, composition, zoning, and alteration, provide valuable insights into mantle composition, metasomatism, and late-stage crystallization (Mitchell, 1986, 1995, 2008; Kamenetsky et al., 2008; Roeder and Schulze, 2008; De Hoog et al., 2010; Mitchell and Tappe, 2010; Pilbeam et al., 2013; Cordier et al., 2015; Sobolev et al., 2015; Nosova et al., 2017).

Forsterite-rich olivine in volcanic rocks carries important information about the mantle source. The modal abundance of olivine in the residual mantle can be estimated from the concentrations of Ni, Mn, and Co in olivine, which are controlled by bulk partition coefficients during mantle melting (Sobolev et al., 2005, 2007; Straub et al., 2008; Foley et al., 2011, 2013; Ghasempour et al., 2014; Dabiri et al., 2018; Borojenie et al., 2025). The concentrations of other trace elements (Ca, Ti, Li, Zn) in olivine, mainly determined by their original content in the source, can be used to identify the nature of metasomatic sources (Prelević and Foley, 2007; Foley et al., 2011, 2013; Prelević et al., 2013; Rooney et al., 2020).

The Eocene volcanic suite in north Ardebil provides valuable insights into mantle dynamics and melt evolution processes beneath NW Iran, reflecting subduction-related magmatism during the Cenozoic. Previous studies have introduced calc-alkaline volcanic sequences dominated by olivine basalts to andesites, which display geochemical evidence of magma mixing and derivation from metasomatized mantle sources (e.g., Vasigh, 2016; Soltanmohammadi et al., 2018; Yazdi et al., 2019; Ahmadzadeh et al., 2023; Salehpour et al., 2025). While whole-rock geochemical data have established the broad subduction zone affinity of these volcanic rocks, significant uncertainties remain about the nature of mantle source heterogeneities and the physicochemical processes that

control melt evolution. In particular, a detailed understanding of the mineralogical and geochemical evolution, especially how olivine composition can be used to trace mantle processes and metasomatic alterations, is still limited. To address these gaps, this study presents high-precision mineral chemistry data for olivine phenocrysts from the north Ardebil Eocene volcanic suite. Our results provide new insights into the primary melt composition and evolutionary pathways of mantle-derived melts in this region.

2. Geological Background

The investigated volcanic region, situated north of Ardebil in NW Iran (Fig. 1), lies within the central segment of the Alpine-Himalayan orogenic belt—a vast tectonic domain formed by the ongoing convergence of the Eurasian and Arabian plates. This region is part of the broader Cenozoic magmatic province of NW Iran, characterized by extensive Eocene volcanic and plutonic activity associated with the subduction of the Neotethys oceanic lithosphere beneath the Iranian continental margin (Berberian and King, 1981; Alavi, 1994; Agard et al., 2005).

During the Eocene, NW Iran experienced widespread magmatism resulting from the northward subduction of the Neotethys oceanic lithosphere. This subduction initiated a complex interplay of arc-related volcanism, crustal extension, and mantle metasomatism. The region is structurally controlled by NW–SE trending faults and is bounded by major tectonic units, including the Sanandaj-Sirjan Zone to the southwest and the South Caspian Basin to the north (Allen et al., 2004; Hassanzadeh and Wernicke, 2016; Mazandarani et al., in press). The Eocene volcanic rocks of north Ardebil are part of the Alborz-Azarbaijan magmatic belt, which extends across NW Iran and is typified by calc-alkaline to shoshonitic volcanic suites (e.g., Castro et al., 2013; Honarmand et al., 2024; Elmi et al., 2025; Abdolahadi et al., 2025). The diversity of magma types produced during Eocene volcanism in NW Iran reflects a complex array of mantle melting processes, likely involving multiple source domains.

The volcanic sequence in our studied region predominantly comprises Eocene-aged basaltic to andesitic flows, pyroclastic deposits, and associated volcaniclastic sediments. These volcanic rocks uncomfortably overlie older Mesozoic sedimentary strata and are locally intruded by coeval Eocene granitoids and mafic dykes (Vasigh, 2016; Fadaeian et al., 2022).

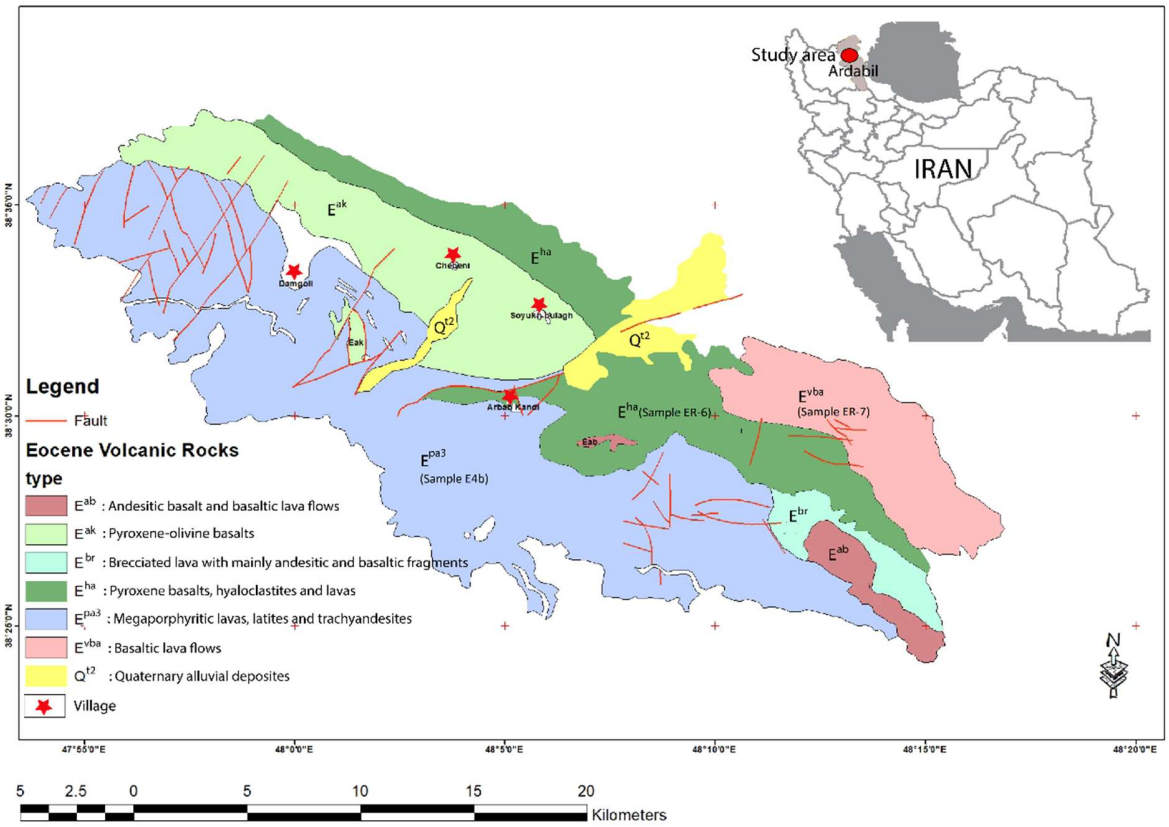

Figure 1. Simplified geological map of Eocene volcanic rocks in the north of Ardabil, showing the approximate locations of samples collected for this study. The figure is modified after Babakhani et al. (1991), Khodabandeh et al. (1997), and Abbasi et al. (2005).

3. Analytical methods

During fieldwork, approximately 100 volcanic rock samples were collected from the study area. A total of 40 samples were prepared as polished thin sections at the University of Tabriz, Iran, for petrographic studies. Among these thin sections, three basaltic samples containing the highest abundance of olivine crystals were selected for detailed electron probe microanalysis (EPMA). Prior to analysis, the samples were re-polished to a standard thickness of 30 microns at the University of Geneva, Switzerland.

Major element compositions of olivine phenocrysts in the selected basaltic samples were analyzed using a JEOL JXA-8530F HyperProbe electron microprobe at the Microprobe Laboratory of the University of Lausanne (UNIL), Switzerland. To ensure representative characterization, over 110 analytical points were measured on olivine crystals. EPMA conditions included an accelerating

voltage of 20 kV, a beam current of 100 nA, and a focused beam diameter of 5 µm. Quantified oxides included SiO_2, FeO, MnO, MgO, NiO, and CaO. Calibration employed a combination of natural and synthetic standards tailored to each element to ensure analytical accuracy and precision. Natural mineral standards such as anorthite (Al_2O_3), wollastonite (CaO, SiO_2), rhodonite (MnO), fayalite (FeO), and albite (Na_2O) were used alongside synthetic oxides, including NiO and TiO_2. These standards were selected to closely match the mineral matrix of olivine, minimizing matrix effects during WDS (Wavelength Dispersive Spectrometry) measurements. Background corrections and analytical parameters followed established CITZAF protocols for quantitative EPMA data reduction.

Preparation for whole-rock XRF analysis was conducted at the University of Geneva (UNIGE), Switzerland. Selected samples for whole-rock analyses were carefully crushed using an agate mortar and pestle to obtain homogenized fine powders. Whole-rock major element contents (SiO_2, TiO_2, Al_2O_3, Fe_2O_3, MnO, MgO, CaO, Na_2O, K_2O, Cr_2O_3, and NiO) were measured by X-ray fluorescence (XRF) at the University of Lausanne. The analyses were performed using a wavelength-dispersive PANalytical AxiosmAX spectrometer fitted with a 4 kW Rh X-ray tube and conducted on fused disks prepared from 1.2 g of calcined sample powder mixed with 6 g of lithium-tetraborate (1:5 mixture). The standard XRF calibration is based on 21 international silicate rock reference materials. The reported data are initially on a loss on ignition (LOI)-free basis and then recalculated to include the LOI (dilution of the LOI-free data).

Whole-rock geochemical analyses were conducted on calibrated fusion discs. Trace elements were measured using an Element XR sector-field ICP-MS (Thermo Scientific) connected to a RESOlution-SE 193 nm laser ablation system featuring an S155 two-volume ablation cell (Australian Scientific Instruments) at the Institute of Earth Sciences, University of Lausanne. The laser ablation was performed under conditions of 10 Hz repetition rate, 9 J/cm² fluence, and a 100 µm spot size diameter. Calibration of relative sensitivity factors was achieved using the NIST SRM 612 soda-lime-silica glass as the primary standard, while the USGS BCR-2g glass served as a secondary quality control standard (Jochum et al., 2011). Internal standardization relied on calcium concentrations obtained from prior XRF measurements. The resulting data were processed using the LAMTRACE software (Jackson, 2008), with detection criteria adapted following Ulianov et al. (2012).

4. Petrography

Based on petrographic studies, the dominant rock type in the studied volcanic suite is basalt. Although these rocks have a basaltic composition, they show variations in the modal abundance of main minerals, as well as differences in crystal size and texture. Considering these petrographic differences, we classify the rocks into three categories: pyroxene-phyric basalt (Sample ER-6), basalt (Sample ER-7) and trachybasalt (Sample E4b). These volcanic rocks commonly show a porphyritic texture, with large, well-formed crystals of clinopyroxene, olivine, and plagioclase set within a fine-grained groundmass. The larger crystals include both phenocrysts, interpreted as having crystallized from the melt, and xenocrysts, likely inherited from the lithospheric mantle or crust. This interpretation is supported by olivine zoning and equilibrium relationships, discussed in later sections. Clinopyroxene crystals commonly host apatite inclusions, which may reflect crystallization in a deeper or earlier magmatic environment, distinct from the host melt. This texture is typical of mantle-derived xenoliths and supports a xenolithic origin (e.g., Shaw, 2024). Olivine and plagioclase phenocrysts are euhedral to subhedral and typically crystallized from the melt. Sanidine occurs as an accessory mineral in the groundmass of trachybasalt, appearing as small, rounded and lath-shaped grains that likely represent a late-stage, K-rich groundmass phase rather than an early-equilibrium crystallizing phase. Opaque minerals, probably magnetite or ilmenite, are scattered throughout the groundmass.

Pyroxene-phyric basalts (Figs. 2a, 2d, and 2g) display a well-developed porphyritic texture, with abundant clinopyroxene crystals (>30%) along with olivine and plagioclase phenocrysts in a fine-grained groundmass. Clinopyroxene appears as subhedral to euhedral crystals, both isolated and in glomeroporphyritic aggregates (Fig. 2d). Some clinopyroxene crystals show compositional and sector zoning and commonly contain apatite inclusions, indicating xenocrystic origin. Olivine crystals vary from euhedral to subhedral, are often rounded, and partly altered to iddingsite along fractures. Plagioclase occurs mostly as lath-shaped crystals with polysynthetic twinning and zoning, forming a significant part of the groundmass. Basalts (Figs. 2b, 2e and 2h) show seriate to porphyritic textures, with a continuous range of crystal sizes from microphenocrysts to groundmass grains. The main phenocrysts are clinopyroxene, olivine, and plagioclase, with apatite inclusions hosted in clinopyroxene. The groundmass consists of fine-grained clinopyroxene, plagioclase, olivine and opaque minerals. In basalt, although the amount of olivine is lower, the

olivines are better developed (more euhedral) than in pyroxene-phyric basalt. Trachybasalt (Figs. 2c, 2f and 2j) are characterized by porphyritic and trachytic textures. These rocks form massive, fine-grained volcanic outcrops (Fig. 2c). Under the microscope (Fig. 2f), they composed of abundant, large clinopyroxenes (subhedral to euhedral), along with olivine and plagioclase phenocrysts, in a finer groundmass of smaller plagioclase laths and minor sanidine. The plagioclase laths, which show a sub-parallel alignment, along with the sanidine crystals, form the trachytic texture in the groundmass. Sanidine is present as smaller, rounded grains, some of which appear resorbed, indicating partial dissolution back into the melt. Opaque minerals, likely magnetite or ilmenite, are scattered throughout the sample as small anhedral grains.

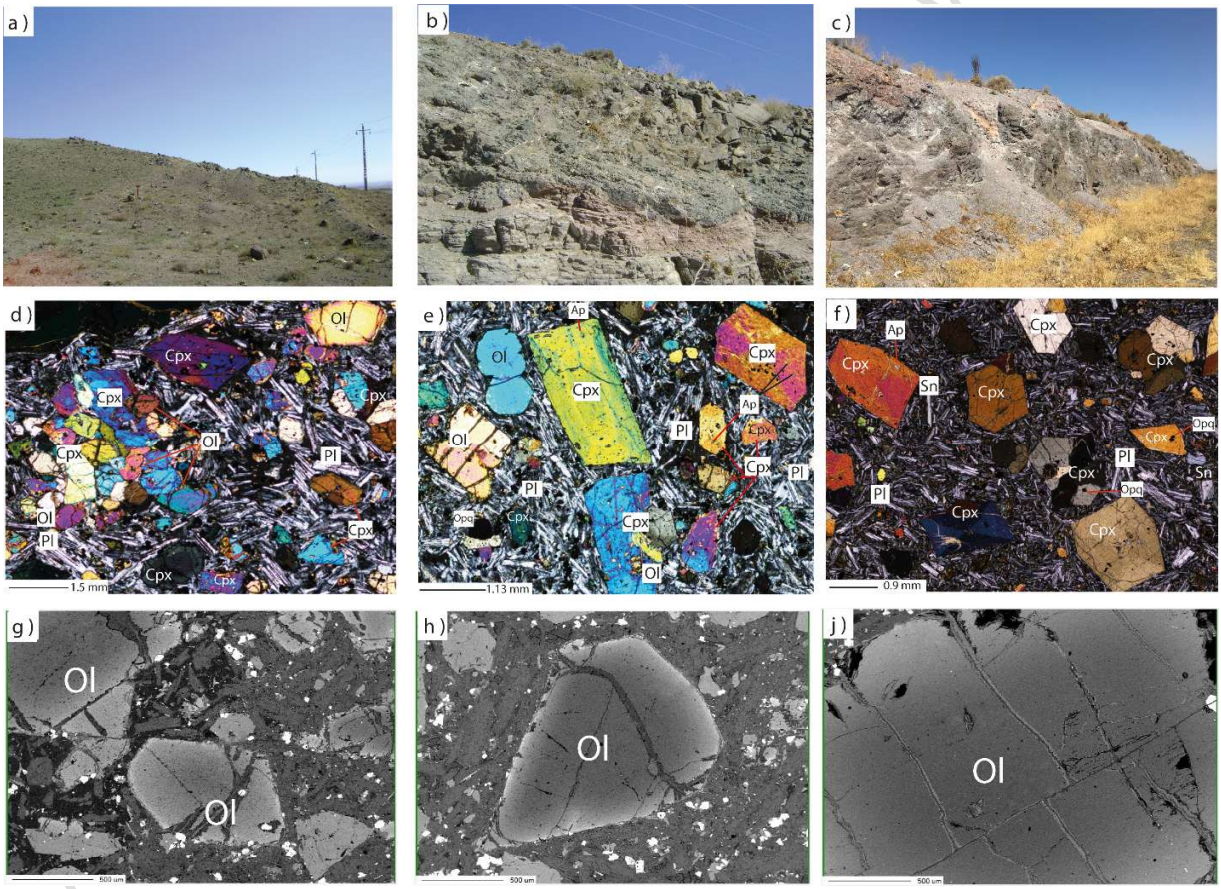

Figure 2. Field, petrographic, and BSE images of Eocene volcanic rocks from north of Ardabil, NW Iran. (a–c) Outcrop views of Pyroxene-phyric basalts (a), Basalt (b), and Trachybasalt (c). (d–f) Cross-polarized photomicrographs showing typical mineral assemblages: clinopyroxene (Cpx), olivine (Ol), plagioclase (Pl), sanidine (San), and apatite (Ap) (Whitney and Evans, 2010) and studied rocks: Pyroxene-phyric basalt (d), Basalt (e) and Trachybasalt (f). (g–j) BSE images of olivine phenocrysts with different zoning patterns and textures in the studied basaltic rocks.

5. Olivine texture

The rocks we studied are porphyritic with a fine-grained groundmass and typically contain 30-50% phenocrysts. The phenocrysts consist mainly of clinopyroxene (25-30%) and olivine (10-15%), while plagioclase occurs primarily as fine-grained laths within the groundmass and only minor amounts as phenocrysts. Olivine crystals (>600 μm in length) can be divided into four chemical and textural types. Their relative abundance was determined by point counting on thin sections using JMicrovision and BSE imaging, which showed some differences between these volcanic rocks (Supplementary Table 1).

Type I olivines are the most common olivine variety and display normal compositional zoning. They are present in all three studied rock types (Fig. 3a). These crystals are characterized by broad core zones with high forsterite contents ($Fo_{87–92}$) (Fig. 3a), surrounded by thin rims (30–40 μm thick) that gradually decrease to more Fe-rich compositions (~$Fo_{62–81}$). The core zones also display slightly elevated NiO concentrations, ranging from 0.29 to 0.41 wt%, compared to the depleted rims (Fig. 3a). Type II phenocrysts are dominant in the trachybasalts; they are coarse-grained (900-2000 μm wide) with euhedral to subhedral crystal forms. These crystals are compositionally homogeneous (mostly ~$Fo_{71–78}$) and show no chemical zoning (Fig. 3b).

Type III olivine phenocrysts, which occur only in pyroxene-phyric basalts, are less common than Types I and II. Most of these crystals are anhedral to subhedral and show normal zoning. They can be identified by their low Mg ($Fo_{59–73}$) and NiO (<0.06 wt%) contents (Fig. 3c). Despite the compositional range in this group, the variations inside single crystals ($Fo_{63–73}$) are much smaller than the variation between different crystals. These olivines likely formed from more evolved magmas. Type IV olivines are the least abundant and are found almost exclusively in the basalt (Sample ER-7). These smaller crystals (around 500 μm) are generally subhedral to anhedral and display oscillatory zoning (Fig. 3d). They have a Mg-rich (Fo_{85-88}) mantle zone with slightly more NiO compared to the core zones (Fig. 3d). Their outermost rims are less magnesian (Fo_{67-77}).

Most olivine crystals observed in the studied volcanic rocks are subhedral and commonly show resorption textures along their rims (Figs. 3a and 3d), suggesting partial dissolution or interaction with the host melt during magmatic evolution. In trachybasalts, olivine phenocrysts are typically larger than those found in pyroxene-phyric basalts and basalts (Figs. 2j and 3a).

Textural observations show that olivine crystals generally display normal compositional zoning, characterized by cores with higher forsterite (Mg-rich) contents that progressively decrease toward the rims. Correspondingly, NiO concentrations decrease toward the rims, while CaO and MnO concentrations increase toward the crystal margins (Figs. 3a–d).

Low NiO contents are typical for most olivine populations, except for the Type I olivines, which display significantly higher NiO concentrations (0.29–0.41 wt%) and distinct compositional signatures compared to other olivine populations within the rock. These differences suggest variations in their crystallization environments or histories.

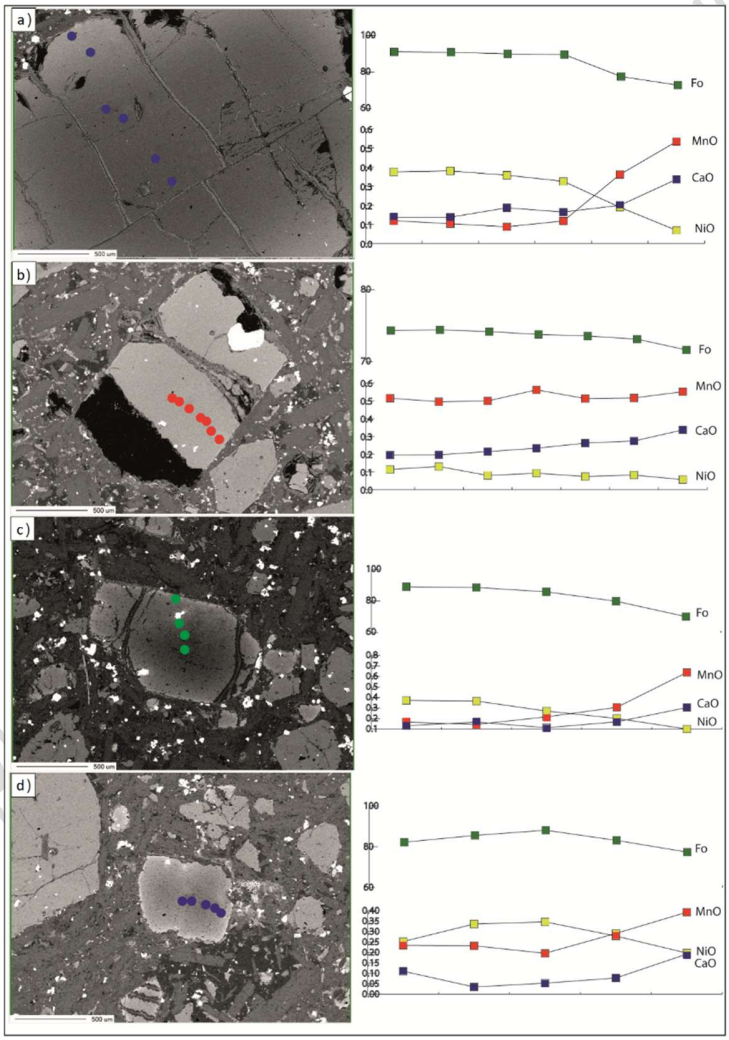

Figure 3. BSE images and chemical profiles of representative olivine phenocrysts from this study. (a–d) BSE images (left) and corresponding core-to-rim compositional variation (right) for four olivine types, showing variations in forsterite (Fo), MnO, CaO, and NiO contents.

6. Results

The detailed analytical results are presented in the Supplementary Table 2.

6.1. Whole-rock major element geochemistry

Whole-rock major element geochemistry was analyzed in three samples, a pyroxene-phyric basalt, a basalt, and a trachybasalt (Samples ER-6, ER-7 and E4b, respectively), for which olivine chemistry has also been analyzed (representative analyses in Table 2). It is important to note that these samples are highly phyric bulk rocks containing xenocrysts; therefore, their compositions and limited sample size do not precisely represent primary melts. Nonetheless, valuable insights can still be gained from their bulk chemistry.

On the total alkali–silica diagram (Fig. 4a), all three samples are subalkaline. SiO_2 ranging from 50.23 and 52.16 wt%. Furthermore, based on the potassium oxide (K_2O) and silica (SiO_2) diagram, the samples fall within the High-K and shoshonitic fields (Fig. 4b), indicating a potassium-enriched magmatic affinity. Loss on Ignition (L.O.I) for basalt and pyroxene-phyric basalt is low (<1.6 wt%), whereas the trachybasalt shows a higher L.O.I of 2.57 wt%. The studied samples represent slightly evolved basalts, with MgO ranging from 5.8 to 9.11 wt% and Mg# values between 40.78 and 44.01. Although the samples generally have low TiO_2 concentrations (<2 wt%), it is notable that the trachybasalts exhibit higher TiO_2 than the other two samples at comparable MgO levels.

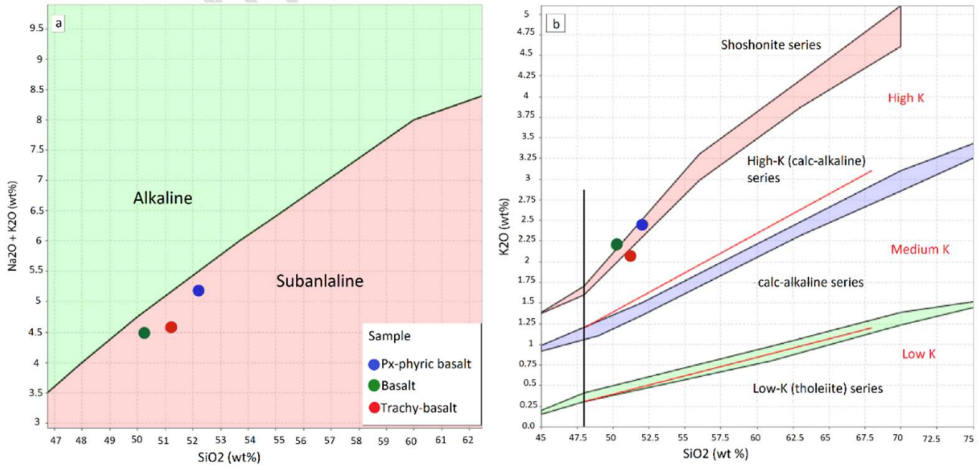

Figure 4. (a) Alkaline/subalkaline classification diagram (after Irvine and Baragar, 1971). (b) Subdivision of subalkalic volcanic rocks based on K_2O versus SiO_2 (wt%) (after Peccerillo and Taylor, 1976).

6.2. Trace elements geochemistry

Fig. 5a displays whole-rock, primitive mantle-normalized trace element patterns of the studied samples, presented according to increasing compatibility of the elements. All samples are characterized by strong enrichment in large-ion lithophile elements (LILE) such as Cs, Rb, Ba, Th, and a pronounced positive anomaly in Pb, relative to the primitive mantle. In contrast, they show marked negative anomalies in high field strength elements (HFSE), including Nb, Ta, P and Ti, relative to light rare earth elements (LREE) (Fig. 5a). The depletion of Nb and Ta is a distinctive feature observed in the studied samples. Enrichment in LILE combined with HFSE depletion is consistent throughout the dataset.

Primitive mantle-normalized rare earth element (REE) patterns are shown in Fig. 5b. The samples reveal strong enrichment in LREE relative to HREE, with flat middle to heavy REE (MREE–HREE) profiles. None of the samples display significant Eu anomalies. High LREE/HREE ratios are particularly evident in the High-K samples analyzed in this study. All samples show LILE enrichment and steep LREE/HREE ratios consistent with a subduction-related arc environment.

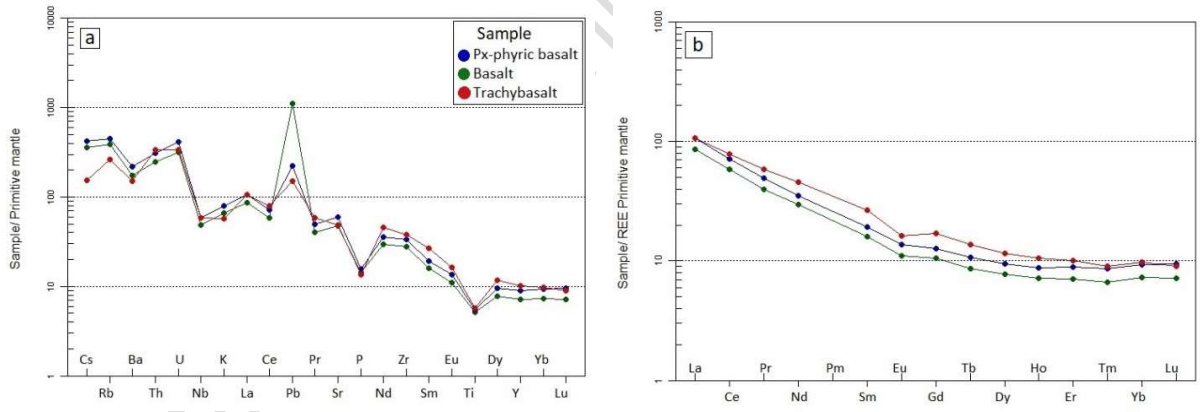

Figure 5. (a) Primitive mantle-normalized spider diagram showing trace element patterns for studied volcanic rocks (normalization values from McDonough and Sun, 1995). (b) Primitive mantle-normalized rare earth element (REE) diagram (normalization values from McDonough and Sun, 1995).

6.3. Olivine chemical compositions

The olivine crystals in all studied samples show a wide range of compositions, with Fo values (Fo = 100 × Mg/ (Mg + Fe), cation ratio) ranging between 59.0 and 92.5, MnO contents from 0.07 to 0.9 wt%, NiO from 0.03 to 0.43 wt%, and CaO from 0 to 0.84 wt% (Fig. 6). We interpret olivine cores with Fo contents greater than 90 (Fo > 90) as xenocrysts, based on a sharp chemical

difference between the cores and their rims, which is inconsistent with normal magmatic zoning. For example, some crystals show core compositions up to Fo~91, while the rims drop to Fo~72 (ΔFo > 19) (Fig. 3a; Table 1). This interpretation is further supported by Fig. 7. These high-Fo (>90) olivines contain relatively high NiO (up to 0.42 wt%), with NiO gradually decreasing toward their rims. NiO content also shows a strong positive correlation with Fo content (Fig. 6a). In contrast, the phenocrystic olivines display a broader range of Fo values but usually have lower Mg contents and higher MnO (up to 0.90 wt%) and CaO concentrations (Figs. 3 and 6b, 6c; Table 1).

Fo content in the olivine cores varies significantly within the three studied rock types, ranging from 60 to 92 in py roxene-phyric basalt, 78 to 92 in basalt, and 72 to 91 in trachybasalt. The more Mg-rich olivines contain low MnO contents (around 0.08 wt%; Fig. 6b), whereas the more Fe-rich phenocrysts have higher MnO contents, up to 0.90 wt% (Table 1). In both groups, a negative correlation with Fo content is observed (Fig. 6b). Calcium concentration is lowest in the Mg-rich olivines (Fig. 6c). The 100 × Mn/Fe ratio ranges from 0.9 to 1.2 in the Mg-rich, Ni-rich olivines, whereas the more Fe-rich olivines show higher values, ranging from 2.5 to 2.7 (Table 1).

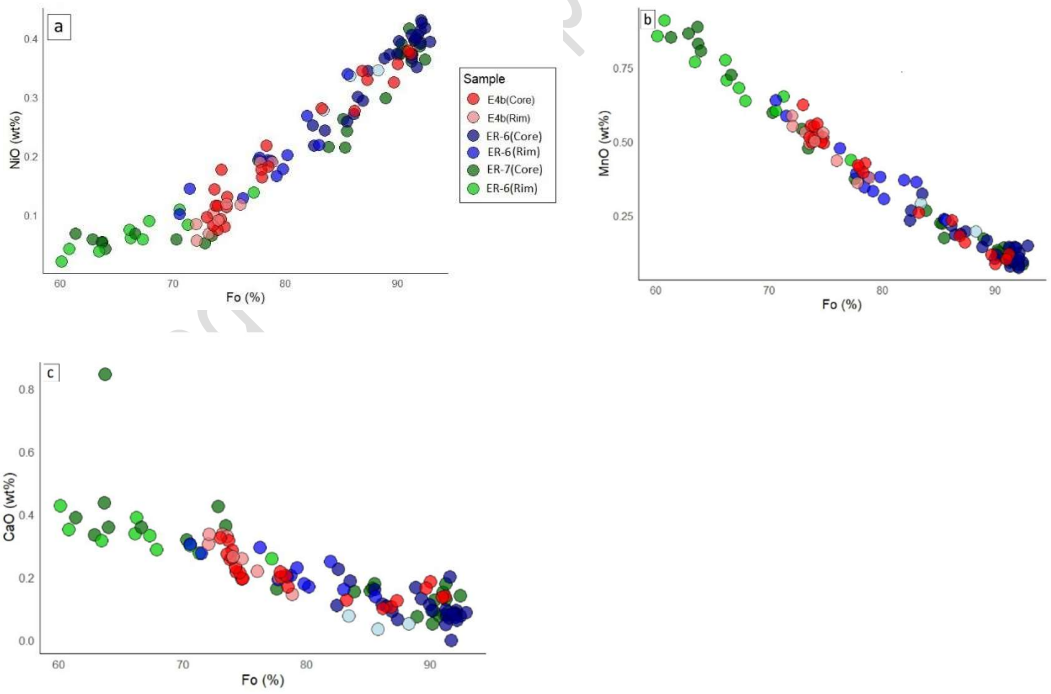

Figure 6. Geochemical variations in olivine compositions illustrating the relationships between Fo (%) and NiO (A), MnO (B), and CaO (C). Data point colors correspond to different rock types and the position of olivines from core to rim within each crystal.

7. Discussion

7.1. Olivine-liquid equilibrium

Experiments have well constrained the Fe/Mg exchange partition coefficient between olivine and basaltic liquid at 0.30 ± 0.03 (Putirka, 2008; Roeder and Emslie, 1970). This coefficient remains constant over a wide range of conditions, except at pressures above 10 kbar (Ulmer, 1989) and in Fe-enriched compositions where the Mg-number is less than 0.25 (Toplis and Carroll, 1995). Mineral-melt equilibrium relationships of this type are best illustrated by plotting whole-rock Mg# against the forsterite content of olivine (Roeder and Emslie, 1970), with the equilibrium field represented as a shaded band extending across the diagram. Fig. 7 shows the relationship between Mg# in whole-rock and the Fo content of olivine phenocrysts for the Eocene volcanic rocks in the north of Ardabil, NW Iran. The green shaded area in this diagram represents the expected Mg# range of olivine phenocrysts equilibrated with coexisting liquids, based on data from tholeiitic basalts (Roeder and Emslie, 1970).

We analyzed core-to-rim compositions of olivine crystals in three basaltic samples. Some olivines show uniform Fo cores with normally zoned rims. Olivine crystals fall into three fields: xenocrysts, equilibrium, and phenocryst/groundmass fields. Cores of type I olivines are largely dominated by xenocrysts, likely formed at greater depths than their host magma. All samples contain olivines with Fo values both above and below the equilibrium field.

Most olivine cores are out of equilibrium, but some cores fall within the equilibrium field (Fig. 7). Samples with core compositions that plot above the equilibrium line have higher Mg content than expected, suggesting they crystallized from more primitive melts or experienced post-entrapment alteration (Sobolev and Chaussidon, 1996; Putirka, 2008). Some olivine phenocrysts show core compositions that plot within equilibrium, while their rims plot below the equilibrium line, reflecting fractional crystallization trends where the rims become enriched in Fe. Samples with core compositions that fall within the equilibrium line are in equilibrium with their melts, implying they formed under conditions consistent with their observed compositions. Olivine cores with Fo < 73 plot just below equilibrium, suggesting they crystallized from more evolved or Fe-enriched melts.

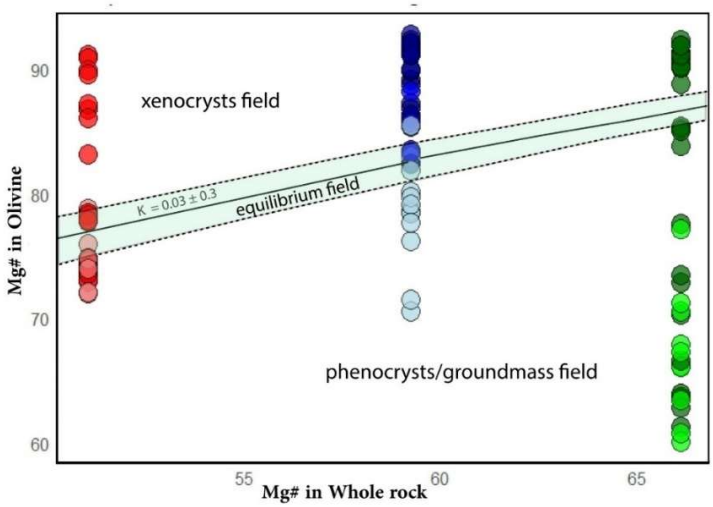

Figure 7. Plot of the relationship between bulk-rock Mg# values and olivine Fo contents. Mg# is defined as $Mg^{2+}/(Mg^{2+} + Fe^{2+})$ and calculated under the assumption of $Fe^{2+}/Fe\_total = 0.9$ for the whole-rock composition, with all Fe in olivine considered as Fe^{2+}. Equilibrium conditions are represented by K_d(Fe-Mg) values of 0.30 ± 0.03 (Roeder and Emslie, 1970).

7.2. Olivine Composition as a Tool for Determining Origin

Determining the origin of chemical and lithological heterogeneity in the mantle source (peridotite, pyroxenite, or their hybridization) is important for understanding the petrogenesis of the volcanic rocks (Sobolev et al., 2007; Herzberg et al., 2014; Elkins et al., 2019). Melts generated from peridotitic and pyroxenitic mantle under similar temperature and pressure conditions have distinct major and trace element compositions, and olivines crystallized from these melts also show different compositions (Sobolev et al., 2005, 2007).

Experimental studies (e.g., Yang et al., 2016) have shown that basaltic melts derived mainly from a pyroxenite mantle source show subtle differences in major and trace element geochemistry compared to melts from a peridotite source. The concentrations of elements such as Ni, Ca, and Mn in parental melts are mainly controlled by their partition coefficients during mantle melting. Specifically, the distribution of Ni and Mn between olivine and melt is strongly influenced by pressure, temperature, and melt composition (Matzen et al., 2013). For instance, these studies indicate that high-pressure melting of peridotite results in an increased Ni partition coefficient between olivine and melt, producing partial melts enriched in Ni and depleted in Mn relative to the residue. The similar behavior of Mn^{2+} and Fe^{2+} during partial melting of ultramafic rocks leads

to a stable Mn/Fe ratio that remains largely unaffected by melting or crystal fractionation processes (Humayun et al., 2004).

The Ni and Ca concentrations in olivine phenocrysts are important indicators of basaltic magma sources (Sobolev et al., 2005, 2007). Applying these geochemical tools to the Eocene volcanic rocks of north Ardabil reveals a complex magmatic history evolution involving both mantle melting and crustal differentiation. Olivine cores from the pyroxene-phyric basalts and xenocrystic olivines (shown with open circles in all figures) that identified based on their high Fo contents (Fo > 90), sharp core–rim compositional gaps (ΔFo > 19), plot within the field of 'olivines from partial melts of Stage 2 pyroxenite' on the Ni-Fo diagram (Fig. 8a). This, along with their relatively low Ca concentrations (Fig. 8b) and core compositions that fall outside the equilibrium field defined by the host melt, provides direct evidence for a pyroxenite-derived melt component in the mantle source.

Subsequent magmatic evolution is recorded in the phenocryst populations from all three rock types. These phenocrysts show a clear fractional crystallization trend, extending to lower Fo and Ni contents (Ni ~270-4000 ppm). The depletion in Ni is consistent with long fractional crystallization of olivine. Furthermore, the phenocrysts are systematically enriched in Ca compared to the xenocrystic and core populations in the px-phyric basalt (Fig. 8b). This elevated Ca content in olivine often shows crystallization from Ca-enriched melts, not residual mantle. This is linked to fertile mantle sources rich in clinopyroxene, which is the main carrier of Ca in the mantle. Consequently, olivine crystallizing from such melts acquires higher Ca content (Toplis and Carroll, 1995). Such characteristics are common in MORB and arc magmas, where mantle source fertility or melting processes produce Ca-enriched melts (Rollinson, 1993; Borghini et al., 2023).

Fe/Mn ratios in the phenocrysts (Fig. 8c) are generally below 60 and similar to peridotite melts. However, their coexistence with high Mn contents (Fig. 8d) and the pyroxenitic signature of some early olivines suggest that the low Fe/Mn ratios are not a reliable indicator of a peridotitic source. Instead, the integrated geochemical signature, such as pyroxenite-like olivine cores followed by a fractional crystallization trend of High-Ca, Low-Fe/Mn phenocrysts, is well explained by the melting of a hybrid mantle source. This source was likely a peridotitic mantle that was metasomatized by melts derived from pyroxenite. Its chemical signature was subsequently

modified by extensive fractional crystallization within the crust (Herzberg et al., 2016; Sobolev et al., 2007).

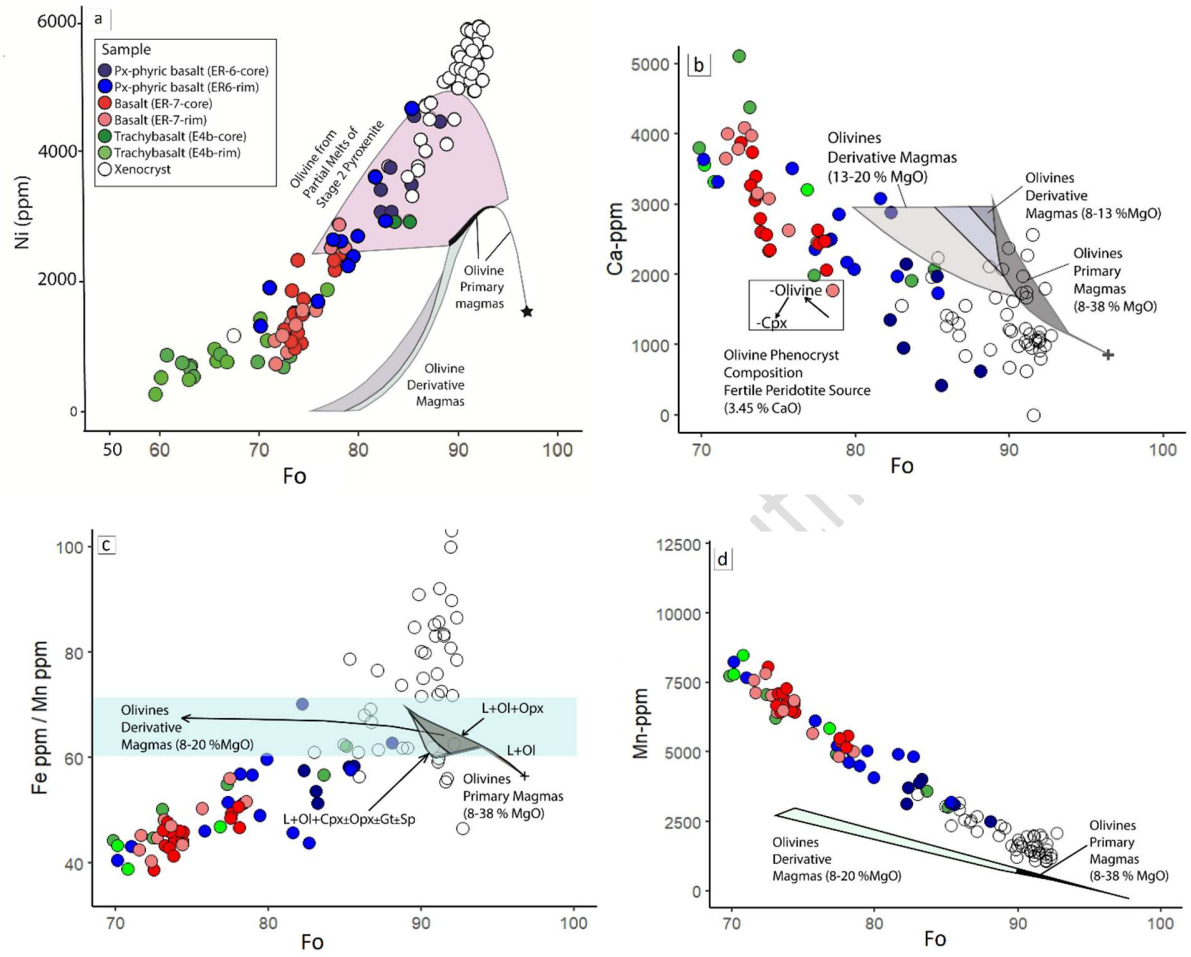

Figure 8. Variations of Ni (a), Ca (b), Fe/Mn (c), and Mn (d) against Fo values of olivines in the Eocene volcanic rocks of north Ardabil. Primary magmas from partial melts of fertile peridotite contain 8–38 wt% MgO. Horizontal and vertical patterned areas represent the calculated compositions of olivines from olivine-fractionated derivative liquids. The pink field in (a) represents olivines from partial melts of Stage 2 pyroxenite (Herzberg, 2011).

7.3. Peridotite versus Pyroxenite: Tracing the Mantle Source

The chemical signature of olivine with Fo content above 90 is an important indicator of the mantle source from which host basalts originate (Sobolev et al., 2007; Herzberg et al., 2014). However, interpretations become more complex when olivine phenocrysts show Fo values below 90, since fractional crystallization significantly changes their composition (Herzberg et al., 2014, 2016). In our samples, olivine phenocrysts range from Fo 59 to 88 (Fig. 3), reflecting such modification.

Petrological modelling is useful for elucidating the impact of fractional crystallization on magma compositions, but it requires an assumed primary magma composition. Typical primary melt calculations often focus on major elements and may omit trace elements such as Ni, which is critical for distinguishing between peridotite and pyroxenite mantle sources. Additionally, the presence of abundant clinopyroxene phenocrysts in the studied samples complicates estimating the primary magma composition. Therefore, we interpret our whole-rock and olivine data by comparing them with representative whole-rock geochemical datasets from the GEOROC database (https://georoc.eu/georoc/new-start.asp).

We plotted the studied samples on the CaO–MgO diagram from Herzberg and Asimow (2008), where the equation $CaO = 13.81 - 0.274 \times MgO$ serves as a compositional boundary between melts derived from peridotite and those potentially sourced from pyroxenite. In the studied samples, basalts with high MgO contents plotted within the peridotite melt field (Fig. 9a), indicating that these basalts likely crystallized primarily olivine. In contrast, pyroxene-phyric basalt and trachybasalt fall within the pyroxenite melt field (Fig. 9a). However, the low-CaO olivines in these samples also show low MgO contents, and their CaO–MgO compositions broadly follow the crystallization trends of peridotite-derived melts (liquid–olivine+cpx+plag). Additionally, the pyroxene-phyric basalt shows chemical characteristics more similar to those of subduction-related arcs such as the Andean and Kamchatka Arcs, which display calc-alkaline arc-type signatures formed by fluid-rich mantle melting above subducting slabs (Bindeman et al., 2004; Espanon et al., 2014; Liu et al., 2020; Shu et al., 2022). On the other hand, the trachybasalt composition resembles volcanics from the East African Rift, a rift setting where magmatism is typically driven by extensional tectonics and mantle plume or decompression melting, yielding alkaline to transitional geochemical signatures distinct from arc magmas (Furman, 2007; Castillo et al., 2014; Liu et al., 2020; Cancel Vazquez et al., 2024). This compositional divergence suggests that the volcanic units may record two distinct tectonomagmatic settings or mantle source processes: the pyroxene-phyric basalt likely formed in the Neotethys subduction-related continental arc, whereas the trachybasalt originated in a back-arc environment. Basalts plotting within the peridotite melt field chemically resemble the Emeishan continental flood basalts, which are characterized by enriched incompatible elements and signatures indicative of a mantle plume origin, with a compositional range from tholeiitic to mildly alkaline (Zhang, 2006; Xie et al., 2009).

This similarity supports the interpretation that these basalts formed during the mid- to late Eocene flare-up magmatism in NW Iran (~45–37 Ma), an episode linked to complex geodynamic processes including Neo-Tethyan subduction and slab rollback (Alavi, 1994; Agard et al., 2005; Shafaii Moghadam et al., 2020).

Further, whole-rock FeO/MnO ratios (Herzberg, 2011) are effective discriminants between pyroxenite and peridotite mantle sources. However, the studied basaltic samples have MgO contents >10 wt% (Figs. 9a and 9b), indicating that their compositions have been affected by fractional crystallization. This process can significantly influence FeO/MnO ratios. Despite this, the observed FeO/MnO values (34–37) are clearly lower than those typical of pyroxenitic melts (>60) and fall below the range expected for peridotite-derived melts (50–60). These observations suggest a more evolved melt, likely derived from a peridotitic source.

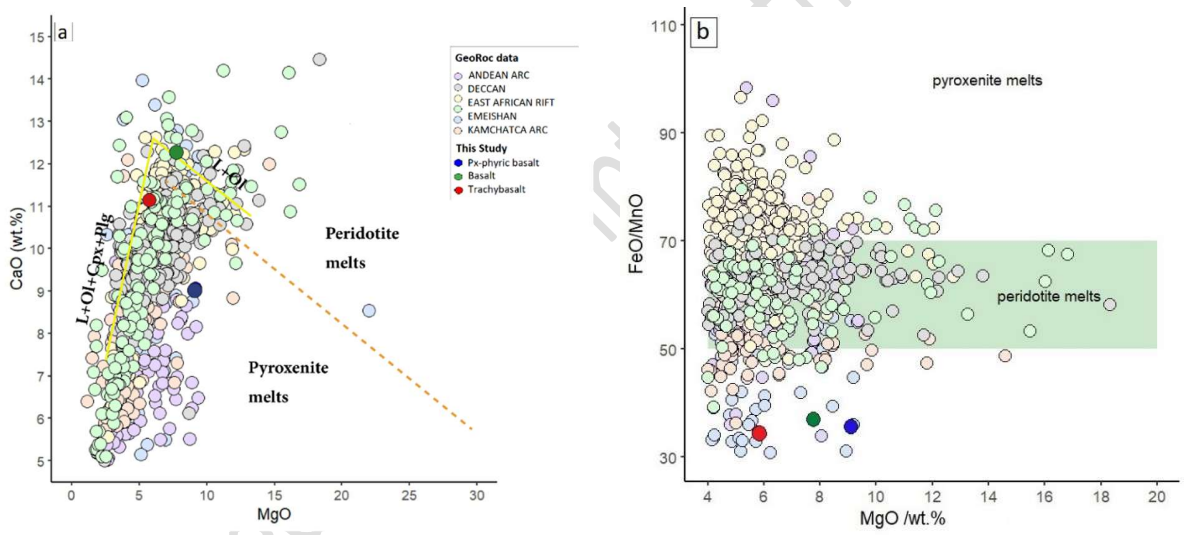

Figure 9. Whole-rock geochemical data compilation for the Eocene volcanic rocks of north Ardebil illustrating indicators of a pyroxenitic source. Blue, red, and green circles represent samples analyzed in this study. (a) MgO (wt.%) versus CaO (wt.%) showing the experimental divide between peridotite and pyroxenite melts (Herzberg and Asimow, 2008). (b) MgO versus FeO/MnO (whole-rock) illustrating the typical field for peridotite melt compositions (Herzberg, 2011). Reference datasets were selected to represent different tectonic environments, including: Convergent Margin: Andean Arc and Kamchatka Arc, Continental Flood Basalt: Emeishan and Deccan and Rift Volcanics: East African Rift

Major and trace element compositions of olivine with high Fo content are commonly used to infer the mantle sources of basaltic magmas (Sobolev et al., 2005, 2007). Except for the olivine cores in sample ER-6 and the xenocrysts, most olivine phenocrysts exhibit chemical compositions

consistent with formation from magmas derived from re-fertilized peridotitic mantle sources (Fig. 8). This interpretation is based on their relatively high Ni contents and moderate CaO values at Fo >85, which deviate from typical fractional crystallization trends and instead align with olivine compositions produced by melting of metasomatized peridotite (Sobolev et al., 2007; Herzberg et al., 2014). In contrast, the xenocrystic olivines and most olivine cores from sample ER-6 (pyroxene-phyric basalt) plot closer to the field of primary magma and pyroxenite melting, suggesting a contribution from relatively less-modified mantle or pyroxenite sources (Fig. 8). In addition, whole-rock geochemical data (Figs. 9b) support a predominantly peridotitic mantle source, while the CaO versus MgO diagram (Fig. 9a) also reveals pyroxenitic contributions. This mixed signal is expected given the limited number of whole-rock analyses available, which naturally results in reduced variability among the samples and restricts the inferences that can be made. Therefore, additional geochemical indicators, including the Ni versus 100 × Mn/Fe diagram in olivine phenocrysts (Sobolev et al., 2007), were used to further constrain the mantle source of the studied rocks. This plot is especially useful because both Ni and Mn/Fe ratios in olivine are sensitive not only to the mineralogy of the source but also to the effects of fractional crystallization and metasomatic modification (Herzberg, 2011; Gall et al., 2021). During fractional crystallization, Ni tends to be incorporated into early-formed olivine, so its concentration decreases in later crystals. In contrast, Mn is moderately incompatible and remains in the melt longer, causing Mn/Fe ratios to rise as crystallization progresses (Herzberg et al., 2014). As a result, olivines formed in more evolved magmas may show lower Ni and higher Mn/Fe values.

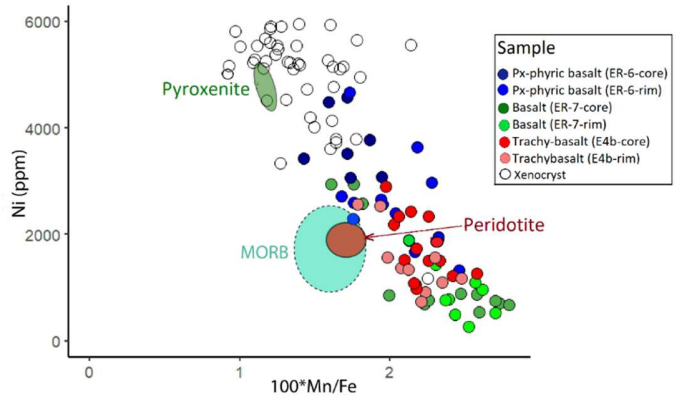

Figure 10. Plots of Ni versus 100 × (Mn/Fe) ratios for olivine crystals. Olivine compositions from MORB and reference fields for olivine crystallized from pyroxenite- and peridotite-derived melts are based on data from Sobolev et al. (2007).

In our dataset, most olivine phenocrysts from basalt and trachybasalt samples plot within or near the peridotite field, suggesting a dominant contribution from a peridotitic mantle source. In contrast, xenocrystic olivines and some cores from the pyroxene-phyric basalt (ER-6) fall closer to the pyroxenite field. This spread in compositions points to a hybrid mantle source beneath north Ardabil, where re-fertilized peridotite is the main contributor, but with variable input from pyroxenitic or sediment-modified domains.

7.4. Insights into Mantle Metasomatism

Nickel enrichment in olivine is closely linked to the mineralogical composition of its mantle source (e.g., Sobolev et al., 2005, 2007; Herzberg, 2011). In convergent margin settings, the addition of silica-rich melts to the mantle wedge often promotes olivine destabilization, resulting in a residue dominated by pyroxene and depleted in olivine (Kelemen et al., 1998). Magmas derived from such modified mantle lithologies tend to crystallize olivine with higher Ni contents than those formed from typical peridotitic sources (Sobolev et al., 2005, 2007; Straub et al., 2008).

Olivine phenocrysts in the analyzed samples are characterized by relatively high concentrations of Ca, Mn, and Ni. While magmatic fractionation generally lowers Ni content and increases Ca and Mn concentrations in olivine, these trends must be interpreted in the context of the Fo content. Most of the olivines in our samples have Fo <90, indicating that fractional crystallization has significantly affected their composition. Therefore, the elevated Mn and Ca concentrations are primarily attributed to magmatic fractionation; however, additional factors such as mantle metasomatism may also influence the observed enrichment of these elements. To further explore mantle metasomatism, we compared our data with published olivine datasets representing MORB, OIB, lamproite, and leucitite compositions (Ammanati et al., 2016). Ammanati et al.'s dataset consists of olivines with Fo >80, whereas our samples include phenocrysts with Fo <80. This difference in Fo content affects trace element ratios such as Ni/Mg and Ca/Fe, which are sensitive to crystallization. As olivine evolves, Ni/Mg ratios decrease and Ca/Fe ratios increase, potentially obscuring source-related signals. Despite this, the 100×Ni/Mg values of olivines from north Ardabil show trends broadly similar to leucitites (Fig. 11a), which are alkaline volcanic rocks commonly associated with carbonatite metasomatism. These elevated Ni/Mg ratios in olivines suggest the incorporation of Ni-rich components derived from such metasomatized mantle melts. However, some samples from ER-6 and xenocrysts are different from this trend and mostly plot

in the lamproite field, suggesting that silicate-rich melts played a major role in the mantle (Figs. 11a and 11b). These variations in olivine Ni/Mg ratios reflect heterogeneity in mantle metasomatic processes beneath the study area. The same trend is observed for xenocrysts and samples from ER-6 in Fig. 11b. However, phenocrysts with low Fo contents (Fo < 90) exhibit Ca/Fe values approaching the lower end of the range commonly linked to carbonated melts. This pattern implies that additional processes, such as crystallization or later metasomatic changes, may have affected these elemental ratios (Figs. 11a and 11b).

Several studies have demonstrated that the addition of subducted sediments significantly influences the petrogenesis of volcanic rocks, as evidenced by elevated Th/La values (up to ~0.3) in the analyzed basaltic samples (Hofmann and White, 1982; Pearce and Peate, 1995; Plank and Langmuir, 1998). Elevated Th/La values in the studied samples (0.36–0.39) strongly suggest that the mantle source was modified by the incorporation of subducted sediments or their derivative melts. This geochemical signature is consistent with magmatic activity in a subduction zone environment, where slab-derived fluids and melts transport sedimentary components into the overlying mantle wedge.

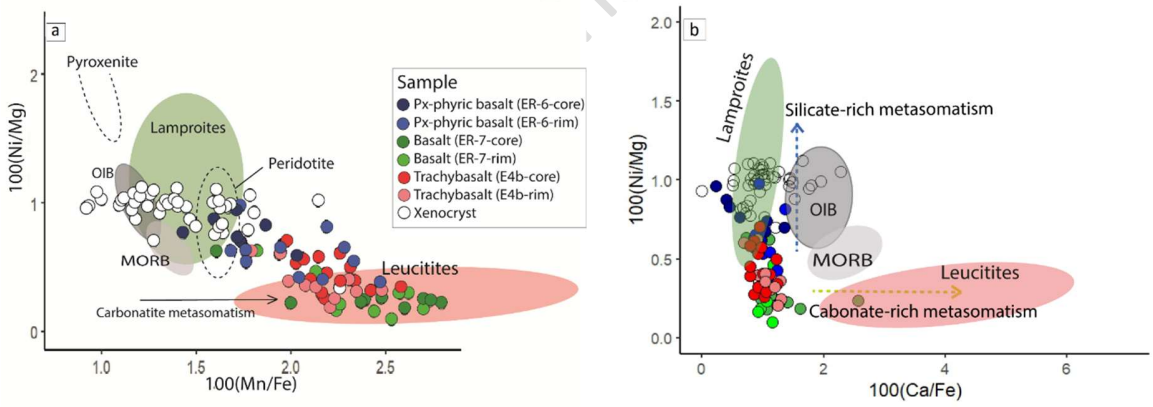

Figure 11. (a) 100 × Mn/Fe and (b) 100 × Ca/Fe plotted against 100 × Ni/Mg in olivines from the studied volcanic rocks analyzed in the present study, with reference data from Ammannati et al. (2016).

Olivines characterized by elevated Ca/Fe and relatively low Ni are expected to result from metasomatism involving carbonate-rich sediment melts (Ammannati et al., 2016; Wölki et al., 2018). However, this pattern is not observed in olivines from north Ardebil. Instead, the analyzed crystals (Fo < 90) display lower Ca/Fe and Ni/Mg values. This discrepancy can be explained by mantle source heterogeneity and complex metasomatic processes. While carbonate-rich sediment

melts typically produce olivines with elevated Ca/Fe and depleted Ni contents, subsequent metasomatism by silicate-rich melts or fluids can partially overprint these geochemical signatures (Ammannati et al., 2016; Wölki et al., 2018). As a result, olivines often display mixed metasomatic characteristics, with reduced Ca/Fe and Ni/Mg ratios compared to those produced by pure carbonate metasomatism.

8. Conclusion

This study provides new insights into the petrogenesis and mantle source characteristics of Eocene volcanic rocks from north Ardebil, NW Iran, based on detailed petrographic observations and high-precision mineral chemistry, with a particular focus on olivine phenocrysts. The studied volcanic suite is dominated by basaltic rocks, which we classify as pyroxene-phyric basalt, basalt, and trachybasalt based on mineral abundance and crystal size. All samples display porphyritic texture.

Olivine phenocrysts in these basaltic rocks show a range of textural and chemical types, including both homogeneous and zoned crystals, with forsterite contents ranging from Fo_{59} to Fo_{92} and variable concentrations of NiO, CaO, and MnO.

Whole-rock geochemical data classify the rocks as subalkaline and High-K calc-alkaline rocks with low TiO_2 and Mg# values. Trace element patterns, including enrichment in Th and La, indicate derivation from a metasomatized lithospheric mantle source, likely influenced by the recycling of subducted sediments during the Eocene and subduction of the Neotethys oceanic lithosphere.

Olivine chemistry reveals enrichment in Ni, Ca, and Mn, suggesting a re-fertilized peridotitic mantle source with pyroxenitic influence. The combination of elevated Ni/Mg and modified Ca/Fe ratios in olivines reflects mixed metasomatic influences from both carbonate- and silicate-rich sediment melts. These metasomatic processes, coupled with magmatic fractionation, have produced hybrid mantle lithologies beneath the volcanic field in north Ardabil during the Eocene.

Whole-rock geochemistry and olivine data together support that the magmatism is linked to subduction-related tectonics, with distinct petrogenetic signs of arc and back-arc environments. This study emphasizes the significance of olivine geochemistry as a tracer for mantle source characteristics and metasomatic processes in complex tectonic settings.

Acknowledgments

This article is extracted from the first author's PhD dissertation. The authors gratefully acknowledge the support of the Swiss National Science Foundation (SNSF) for providing the opportunity to conduct EPMA and ICP-MS analyses.

References

Abbasi S., Khalatbari-Jafari M., Sahbari P. (2005) Geological map of Razi (1: 100,000 scale). Geological Survey of Iran, Tehran.

Abdolahadi A., Sheikhzakariaee S.J., Yazdi A., Mousavi S.Z. (2025) Plio-Quaternary Adakite Genesis and Post-collisional Processes: Whole Rock Constraints and Sr, Nd Isotopic Compositions in Alborz Magmatic Belt, Ardabil, Iran, *Journal of Mining and Environment*, 16(2):737-765. DOI: https://doi.org/10.22044/jme.2024.14781.2801

Agard P., Omrani J., Jolivet L., Mouthereau F. (2005) Convergence history across Zagros (Iran): Constraints from collisional and earlier deformation. *International Journal of Earth Sciences* 94:401–419. DOI: https://doi.org/10.1007/s00531-005-0481-4

Ahmadzadeh G., Mobashergermi M., Ravankhah A. (2023) Petrology, geochemistry and petrogenesis of Eocene volcanic rocks from Khan Ali Darasi, north of Lahrod city, northwest Iran. *Researches in Earth Sciences* 14(1):45–63. DOI: https://doi.org/10.48308/esrj.2023.101419

Alavi M. (1994) Tectonics of the Zagros Orogenic Belt of Iran: New data and interpretations. *Tectonophysics* 229(3–4):211–238. DOI: https://doi.org/10.1016/0040-1951(94)90030-2

Allen M., Jackson J., Walker R. (2004) Late Cenozoic reorganization of the Arabia–Eurasia collision and the comparison of short-term and long-term deformation rates. *Tectonics* 23(2):1–18. DOI: https://doi.org/10.1029/2003TC001530

Ammannati E., Jacob D. E., Avanzinelli R., Foley S. F., Conticelli S. (2016) Low Ni olivine in silica-undersaturated ultrapotassic igneous rocks as evidence for carbonate metasomatism in the mantle. *Earth and Planetary Science Letters* 444:64–74. DOI: https://doi.org/10.1016/j.epsl.2016.03.039

Arjmandzadeh R.,, Sharifi Teshnizi E., Ahmadi A.A., Mahdavi A., Tavsoli S., Dabiri R. (2021) The mineralogy, geochemistry and genesis of Aghol-Messi sedimentary copper-uranium deposit, Tabas block, Central Iran, *Researches in Earth Sciences,* 11(4): 47-70. DOI: https://doi.org/10.52547/esrj.11.4.47

Arndt N. T., Guitreau M., Boullier A. M., Le Roex A., Tommasi A., Cordier P., Sobolev A. (2010) Olivine and the origin of kimberlite. *Journal of Petrology* 51:573–602. DOI: https://doi.org/10.1093/petrology/egp080

Babakhani A. R., Nazer N. H., Amidi M. (1991) Geological map of Lahrood (1: 100,000 scale). Geological Survey of Iran, Tehran.

Berberian M., King G. C. P. (1981) Towards a paleogeography and tectonic evolution of Iran. *Canadian Journal of Earth Sciences* 18(2):210–265. DOI: https://doi.org/10.1139/e81-019

Bindeman I. N., Ponomareva V. V., Bailey J. C., Valley J. W. (2004) Volcanic arc of Kamchatka: A province with high-$\delta^{18}O$ magma sources and large-scale $^{18}O/^{16}O$ depletion of the upper crust. *Geochimica et Cosmochimica Acta* 68(4):841–865. DOI: https://doi.org/10.1016/j.gca.2003.07.009

Borghini G., Fumagalli P., Arrigoni F., Rampone E., Berndt J., Klemme S., Tiepolo M. (2023) Fast REE re-distribution in mantle clinopyroxene via reactive melt infiltration. *Geochemical Perspectives Letters* 26:40–44. DOI: https://doi.org/10.7185/geochemlet.2323

Borojenie T. H., Sheykhzakariaei S.J., Dabiri R., Yazdi A. (2025) Petrogenesis and tectonic implications of Neoproterozoic to Cenozoic A-type granitoids in NW Iran: geochemical and tectonic constraints, *Iranian Journal of Earth Sciences*, 17(4): 1-19. DOI: https://doi.org/10.57647/j.ijes.2025.16894

Cancel Vazquez S. M., Rooney T. O., Brown E. L., Bollinger A., Bastow I. D., Steiner R. A., Kappelman J. (2024) Basaltic pulses and lithospheric thinning—Plio-Pleistocene magmatism and rifting in the Turkana Depression (East African Rift System). *Journal of Geophysical Research: Solid Earth* 129(8): e2024JB029166. DOI: https://doi.org/10.1029/2024JB029166

Castillo P. R., Hilton D. R., Halldórsson S. A. (2014) Trace element and Sr-Nd-Pb isotope geochemistry of Rungwe Volcanic Province, Tanzania: Implications for a Superplume source for

East Africa Rift magmatism. *Frontiers in Earth Science* 2:21. DOI: https://doi.org/10.3389/feart.2014.00021

Castro A., Aghazadeh M., Badrzadeh Z., Chichorro M. (2013) Late Eocene–Oligocene post-collisional monzonitic intrusions from the Alborz magmatic belt, NW Iran: An example of monzonite magma generation from a metasomatized mantle source. *Lithos* 180–181:109–127. DOI: https://doi.org/10.1016/j.lithos.2013.08.009

Cordier C., Sauzeat L., Arndt N. T., Boullier A. M., Batanova V., Barou F. (2015) Metasomatism of the lithospheric mantle immediately precedes kimberlite eruption: New evidence from olivine composition and microstructures. *Journal of Petrology* 56:1775–1796. DOI: https://doi.org/10.1093/petrology/egv054

Dabiri R., Akbari-Mogaddam M., Ghaffari M. (2018) Geochemical evolution and petrogenesis of the eocene Kashmar granitoid rocks, NE Iran: implications for fractional crystallization and crustal contamination processes, *Iranian Journal of Earth Sciences* 10 (1): 68-77.

De Hoog J. C. M., Gall L., Cornell D. H. (2010) Trace-element geochemistry of mantle olivine and application to mantle petrogenesis and geothermobarometry. *Chemical Geology* 270:196–215. DOI: https://doi.org/10.1016/j.chemgeo.2009.11.017

Elkins L. J., Bourdon B., Lambart S. (2019) Testing pyroxenite versus peridotite sources for marine basalts using U-series isotopes. *Lithos* 332–333:226–244. DOI: https://doi.org/10.1016/j.lithos.2019.02.011

Elmi R., Arian M. A., Ashja Ardalan A., Yazdi A. (2025) Petrology of volcanism in the Alasht-Haraz road of the Alborz mountain range, south of Amol (north of Iran), *Iranian Journal of Earth Sciences*, 17(3): 1-16. DOI: https://doi.org/10.57647/j.ijes.2025.16800

Espanon V. R., Chivas A. R., Kinsley L. P. J., Dosseto A. (2014) Geochemical variations in the Quaternary Andean back-arc volcanism, southern Mendoza, Argentina. *Lithos* 208–209:251–264. DOI: https://doi.org/10.1016/j.lithos.2014.09.010

Fadaeian M., Jahangiri A., Ao S., Kamali A. A., Xiao W. (2022) Geochemistry and petrogenesis of shoshonitic dyke swarm in the northeast of Meshkinshahr, NW Iran. *Minerals* 12(3):309. DOI: https://doi.org/10.3390/min12030309

Foley S. F., Jacob D. E., O'Neill H. S. C. (2011) Trace element variations in olivine phenocrysts from Ugandan potassic rocks as clues to the chemical characteristics of parental magmas. *Contributions to Mineralogy and Petrology* 162(1):1–20. DOI: https://doi.org/10.1007/s00410-010-0579-y

Foley S. F., Prelević D., Rehfeldt T., Jacob D. E. (2013) Minor and trace elements in olivines as probes into early igneous and mantle melting processes. *Earth and Planetary Science Letters* 363:181–191. DOI: https://doi.org/10.1016/j.epsl.2012.11.025

Furman T. (2007) Geochemistry of East African Rift basalts: An overview. *Journal of African Earth Sciences* 48(2–3):147–160. DOI: https://doi.org/10.1016/j.jafrearsci.2006.06.009

Gall H., Furman T., Hanan B., Kürkcüoğlu B., Sayıt K., Yürür T., Pickard Sjoblom M., Şen E., Alıcı Şen P. (2021) Post-delamination magmatism in south-central Anatolia. *Lithos* 398–399:106299. DOI: https://doi.org/10.1016/j.lithos.2021.106299

Ghasempour M.R., Ghazi J.M., Biabangard H., Dabiri R. (2014) Petrogenic significance of the Plio-Quaternary Nehbandan mafic lavas, Eastern Iran, *Iranian Journal of Earth Sciences,* 6(2): 133-141.

Giuliani A., Foley S. F. (2016) The geochemical complexity of kimberlite rocks and their olivine populations: A comment on Cordier et al. (Journal of Petrology, 56, 1775–1796, 2015). *Journal of Petrology* 57:927–932. DOI: https://doi.org/10.1093/petrology/egw026

Hassanzadeh J., Wernicke B. (2016) The Neotethyan Sanandaj-Sirjan zone of Iran as an archetype for passive margin-arc transitions. *Tectonics* 35(3):586–621. DOI: https://doi.org/10.1002/2015TC003926

Herzberg C. (2011) Identification of source lithology in the Hawaiian and Canary Islands: Implications for origins. *Journal of Petrology* 52(1):113–146. DOI: https://doi.org/10.1093/petrology/egr015

Herzberg C., Asimow P. D. (2008) Petrology of some oceanic island basalts: PRIMELT2.XLS software for primary magma calculation. *Geochemistry, Geophysics, Geosystems* 9(9):1–29. DOI: https://doi.org/10.1029/2008GC002057

Herzberg C., Cabral R. A., Jackson M. G., Vidito C., Day J., Hauri E. H. (2014) Phantom Archean crust in Mangaia hot-spot lavas and the meaning of heterogeneous mantle. *Earth and Planetary Science Letters* 396:97–106. DOI: https://doi.org/10.1016/j.epsl.2014.03.065

Herzberg C., Vidito C., Starkey N. A. (2016) Nickel–cobalt contents of olivine record origins of mantle peridotite and related rocks. *American Mineralogist* 101(9):1952–1966. DOI: https://doi.org/10.2138/am-2016-5538

Hofmann A. W., White W. M. (1982) Mantle plumes from ancient oceanic crust. *Earth and Planetary Science Letters* 57(1–2):421–436. DOI: https://doi.org/10.1016/0012-821X(82)90161-3

Honarmand M., van der Boon A., Neubauer F., Heberer B., Li Q., Kuiper K. F., Mason P. R. D., Krijgsman W. (2024) Geochemical constraints on the geodynamic setting of Alborz-Azerbaijan Cenozoic magmatism. *Chemical Geology* 645:1–23. DOI: https://doi.org/10.1016/j.chemgeo.2023.121889

Humayun M., Qin L., Norman M. D. (2004) Geochemical evidence for excess iron in the mantle beneath Hawaii. *Science* 306(5693):91–94. DOI: https://doi.org/10.1126/science.1101050

Irvine T. N., Baragar W. R. A. (1971) A guide to the chemical classification of the common volcanic rocks. *Canadian Journal of Earth Sciences* 8(5):523–548. DOI: https://doi.org/10.1139/e71-055

Jackson S. E. (2008) LAMTRACE data reduction software for LA-ICP-MS. In: Sylvester P. (ed) *Mineralogical Association of Canada Short Course Series* 40:305–307. DOI: https://doi.org/10.3749/9780921294801.app01

Jochum K. P., Weis U., Stoll B., Kuzmin D., Yang Q., Raczek I., Jacob D. E., Stracke A., Birbaum K., Frick D. A., Günther D., Enzweiler J. (2011) Determination of reference values for NIST SRM 610–617 glasses following ISO guidelines. *Geostandards and Geoanalytical Research* 35:397–429. DOI: https://doi.org/10.1111/j.1751-908X.2011.00120.x

Kamenetsky V. S., Kamenetsky M. B., Sobolev A. V., Alexander V. G., Sylvie D., Kevin F., Victor V. S., Dmitry V. K. (2008) Olivine in the Udachnaya-East kimberlite (Yakutia, Russia):

Types, compositions and origins. *Journal of Petrology* 49:823–839. DOI: https://doi.org/10.1093/petrology/egm033

Kelemen P. B., Hart S. R., Bernstein S. (1998) Silica enrichment in the continental upper mantle via melt/rock reaction. *Earth and Planetary Science Letters* 164(3–4):387–406. DOI: https://doi.org/10.1016/S0012-821X(98)00233-7

Khodabandeh A., Amini Fazl A., Emami M. H. (1997) Geological map of Ardebil (1: 100,000 scale). Geological Survey of Iran, Tehran.

Liu H., Xiao Y., Sun H., Tong F., Heuser A., Churikova T., Wörner G. (2020) Trace elements and Li isotope compositions across the Kamchatka arc: Constraints on slab-derived fluid sources. *Journal of Geophysical Research: Solid Earth* 125(5): e2019JB019237. DOI: https://doi.org/10.1029/2019JB019237

Matzen A. K., Baker M. B., Beckett J. R., Stolper E. M. (2013) The temperature and pressure dependence of nickel partitioning between olivine and silicate melt. *Journal of Petrology* 54(12):2521–2545. DOI: https://doi.org/10.1093/petrology/egt055

Mazandarani R., Sheikh Zakariaee S.J., Mortazavi, S.M., Yazdi A. (In press) Geodynamics and tectonic setting of volcanic rocks from Tineh to Reineh (Haraz road) in Iran, *Geopersia*, Doi: https://doi.org/10.22059/geope.2025.395984.648823

McDonough W. F., Sun S. S. (1995) The composition of the Earth. *Chemical Geology* 120(3–4):223–253. DOI: https://doi.org/10.1016/0009-2541(94)00140-4

Mitchell R. H. (1986) Kimberlites: Mineralogy, geochemistry, and petrology (442 pp.). *Plenum Press.*

Mitchell R. H. (1995) Kimberlites, orangeites and related rocks (410 pp.). *Plenum Press*. DOI: https://doi.org/10.1007/978-1-4615-1993-5

Mitchell R. H. (2008) Petrology of hypabyssal kimberlites: Relevance to primary magma compositions. *Journal of Volcanology and Geothermal Research* 174(1–3):1–8. DOI: https://doi.org/10.1016/j.jvolgeores.2007.12.024

Mitchell R. H., Tappe S. (2010) Discussion of "Kimberlites and aillikites as probes of the continental lithospheric mantle," by Francis and Patterson (Lithos v. 109, p. 72–80). *Lithos* 115(1):288–292. DOI: https://doi.org/10.1016/j.lithos.2009.10.017

Mollai H., Dabiri R., Torshizian H. A., Pe-Piper G., Wang W. E. (2021) Upper Neoproterozoic garnet-bearing granites in the Zeber-Kuh region from east central Iran micro plate: Implications for the magmatic evolution in the northern margin of Gondwanaland, *Geologica Carpathica* 72 (6): 461-81. DOI: https://doi.org/10.31577/GeolCarp.72.6.2

Nosova A., Dubinina E., Sazonova L. G., Kargin A., Lebedeva N., Khvostikov V., Burmii Z. P., Kondrashov I., Tret'yachenko V. V. (2017) Geochemistry and oxygen isotopic composition of olivine in kimberlites from the Arkhangelsk Province: Contribution of mantle metasomatism. *Petrology* 25(2):150–180. DOI: https://doi.org/10.1134/S0869591117010064

Pearce J. A., Peate D. W. (1995) Tectonic implications of the composition of volcanic arc magmas. *Annual Review of Earth and Planetary Sciences* 23:251–285. DOI: https://doi.org/10.1146/annurev.ea.23.050195.001343

Peccerillo A., Taylor S. R. (1976) Geochemistry of Eocene calc-alkaline volcanic rocks from the Kastamonu area, northern Turkey. *Contributions to Mineralogy and Petrology* 58:63–81. DOI: https://doi.org/10.1007/BF00384745

Pilbeam L. H., Nielsen T. F. D., Waight T. E. (2013) Digestion fractional crystallization (DFC): An important process in the genesis of kimberlites. Evidence from olivine in the Majuagaa kimberlite, southern West Greenland. *Journal of Petrology* 54:1399–1425. DOI: https://doi.org/10.1093/petrology/egt016

Plank T., Langmuir C. H. (1998) The chemical composition of subducting sediment and its consequences for the crust and mantle. *Chemical Geology* 145(3–4):325–394. DOI: https://doi.org/10.1016/S0009-2541(97)00150-2

Prelević D., Foley S. F. (2007) Accretion of arc-oceanic lithospheric mantle in the Mediterranean: Evidence from extremely High-Mg olivines and Cr-rich spinel inclusions from lamproites. *Earth and Planetary Science Letters* 256(1–2):120–135. DOI: https://doi.org/10.1016/j.epsl.2007.01.018

Prelević D., Jacob D. E., Foley S. F. (2013) Recycling plus: A new recipe for the formation of Alpine-Himalayan orogenic mantle lithosphere. *Earth and Planetary Science Letters* 362:187–197. DOI: https://doi.org/10.1016/j.epsl.2012.11.035

Putirka K. D. (2008) Thermometers and barometers for volcanic systems. *Reviews in Mineralogy and Geochemistry* 69(1):61–120. DOI: https://doi.org/10.2138/rmg.2008.69.3

Roeder P. L., Emslie R. F. (1970) Olivine-liquid equilibrium. *Contributions to Mineralogy and Petrology* 29:275–289. DOI: https://doi.org/10.1007/BF00371276

Roeder P. L., Schulze D. J. (2008) Crystallization of groundmass spinel in kimberlite. *Journal of Petrology* 49(8):1473–1495. DOI: https://doi.org/10.1093/petrology/egn034

Rollinson H. R. (1993) Using geochemical data: Evaluation, presentation, interpretation. *Routledge*, London, 384 pp. DOI: https://doi.org/10.4324/9781315845548

Rooney T. O., Girard G., Tappe S. (2020) The impact on mantle olivine resulting from carbonated silicate melt interaction. *Contributions to Mineralogy and Petrology* 175(6):56–71. DOI: https://doi.org/10.1007/s00410-020-01694-0

Salehpour S., Arian M.A., Rad A.J., Zarei Sahamieh R., Yazdi A. (2025) Geochemistry and technomagmatic environment of Eocene volcanic rocks in Yuzbashi Chay region, west of Qazvin (Iran), Iranian Journal of Earth Sciences, 17(1): 1-13. https://doi.org/10.57647/j.ijes.2025.1701.04

Shafaii Moghadam H., Li Q. L., Li X. H., Stern R. J., Levresse G., Santos J. F., Lopez Martinez M., Ducea M. N., Ghorbani G., Hassannezhad A. (2020) Neotethyan subduction ignited the Iran arc and backarc differently. *Journal of Geophysical Research: Solid Earth* 125(4): e2019JB018460. DOI: https://doi.org/10.1029/2019JB018460

Shaw C. S. J. (2024) Clinopyroxenite xenoliths record magma transport and crystallization in the middle and upper crust: A case study from the Rockeskyllerkopf Volcanic Complex, West Eifel, Germany. Journal of Petrology 65(4): egae035. DOI: https://doi.org/10.1093/petrology/egae035

Shu Y., Nielsen S. G., Le Roux V., Wörner G., Blusztajn J., Auro M. (2022) Sources of dehydration fluids underneath the Kamchatka arc. *Nature Communications* 13:4467. DOI: https://doi.org/10.1038/s41467-022-32211-5

Søager N., Portnyagin M., Hoernle K., Holm P. M., Hauff F., Garbeschönberg D. (2015) Olivine major and trace element compositions in southern Payenia basalts, Argentina: Evidence for pyroxenite-peridotite melt mixing in a back-arc setting. *Journal of Petrology* 56:1495–1518. DOI: https://doi.org/10.1093/petrology/egv043

Sobolev A. V., Chaussidon M. (1996) Melt inclusions in minerals as a source of principal petrological information: New data from olivine phenocrysts of basalts and kimberlites. *Petrology* 4(3):209–220.

Sobolev A. V., Hofmann A. W., Kuzmin D. V., Yaxley G. M., Arndt N. T., Chung S. L., Gurenko A. A. (2007) The amount of recycled crust in sources of mantle-derived melts. *Science* 316(5823):412–417. DOI: https://doi.org/10.1126/science.1138113

Sobolev A. V., Hofmann A. W., Sobolev S. V., Nikogosian I. K. (2005) An olivine-free mantle source of Hawaiian shield basalts. *Nature* 434(7033):590–597. DOI: https://doi.org/10.1038/nature03411

Sobolev N. V., Sobolev A. V., Tomilenko A. A., Kovyazin S. V., Batanova V. G., Kuz'min D. V. (2015) Paragenesis and complex zoning of olivine macrocrysts from unaltered kimberlite of the Udachnaya-East pipe, Yakutia: Relationship with the kimberlite formation conditions and evolution. *Russian Geology and Geophysics* 56(1–2):260–279. DOI: https://doi.org/10.1016/j.rgg.2015.01.019

Soltanmohammadi A., Grégoire M., Rabinowicz M., Gerbault M., Ceuleneer G., Rahgoshay M., Bystricky M., Benoit M. (2018) Transport of volatile-rich melt from the mantle transition zone via compaction pockets: Implications for mantle metasomatism and the origin of alkaline lavas in the Turkish–Iranian Plateau. *Journal of Petrology* 59(12):2273–2310. DOI: https://doi.org/10.1093/petrology/egy097

Straub S. M., LaGatta A. B., Martin-Del Pozzo A. L., Langmuir C. H. (2008) Evidence from High-Ni olivines for a hybridized peridotite/pyroxenite source for orogenic andesites from the central Mexican Volcanic Belt. *Geochemistry, Geophysics, Geosystems* 9(3): Q03007. DOI: https://doi.org/10.1029/2007GC001583

Toplis M. J., Carroll M. R. (1995) An experimental study of the influence of oxygen fugacity on Fe-Ti oxide stability, phase relations, and mineral-melt equilibria in ferro-basaltic systems. *Journal of Petrology* 36(5):1137–1170. DOI: https://doi.org/10.1093/petrology/36.5.1137

Ulianov A., Müntener O., Schaltegger U., Bussy F. (2012) The data treatment dependent variability of U–Pb zircon ages obtained using mono-collector, sector field, laser ablation ICP-MS. *Journal of Analytical Atomic Spectrometry* 27(4):663–676. DOI: https://doi.org/10.1039/C2JA10358C

Ulmer P. (1989) The dependence of the Fe^{2+}–Mg cation-partitioning between olivine and basaltic liquid on pressure, temperature and composition: An experimental study to 30 kbars. *Contributions to Mineralogy and Petrology* 101(3):261–273. DOI: https://doi.org/10.1007/BF00375311

Vasigh Y. (2016) Petrogenesis of volcanic rocks from Razei region in Northwest Ardabil, Iran. *Iranian Journal of Earth Sciences* 8(1):69–77.

Whitney D. L., Evans B. W. (2010) Abbreviations for names of rock-forming minerals. *American Mineralogist* 95:185–187. DOI: https://doi.org/10.2138/am.2010.3371

Wölki D., Haase K., Schoenhofen M., Beier C., Regelous M., Krumm S. H., Günther T. (2018) Evidence for melting of subducting carbonate-rich sediments in the western Aegean Arc. *Chemical Geology* 483:463–473. DOI: https://doi.org/10.1016/j.chemgeo.2018.03.014

Xie S., Keays R. R., Xiao L., Huo Q., Ihlenfeld C. (2009) Platinum-group element geochemistry of the continental flood basalts in the central Emeishan Large Igneous Province, SW China. *Chemical Geology* 260(3–4):246–261. DOI: https://doi.org/10.1016/j.chemgeo.2009.01.021

Yang Z. F., Zhou J. H., Qian Q. (2016) On the chemical markers of pyroxenite contributions in continental basalts in Eastern China: Implications for source lithology and the origin of basalts. *Journal of Petrology* 157(1–3):18–31. DOI: https://doi.org/10.1016/j.earscirev.2016.04.001

Yazdi A., Ashja-Ardalan A., Emami M.H., Dabiri R., Foudazi M. (2019) Magmatic interactions as recorded in plagioclase phenocrysts of quaternary volcanics in SE Bam (SE Iran), *Iranian Journal of Earth Sciences* 11(3): 215-224. https://doi.org/10.30495/ijes.2019.667379

Zhang Z., Mahoney J. J., Mao J., Wang F. (2006) Geochemistry of picritic and associated basalt flows of the western Emeishan flood basalt province, China. *Journal of Petrology* 47(10):1997–2019. DOI: https://doi.org/10.1093/petrology/egl034